


Deformation and burst of a liquid droplet with viscous surface moduli in a linear flow field

Natasha Singh  and Vivek Narsimhan**Davidson School of Chemical Engineering, Purdue University, 480 Stadium Mall Drive, West Lafayette, Indiana 47907, USA*

(Received 3 December 2019; accepted 5 May 2020; published 1 June 2020)

Suspensions of fluid particles with complex interfacial architecture (for instance, capsules, vesicles, polymersomes, lipid bilayers, and emulsions embedded with certain surface-active agents and surfactants) find an immense number of applications in the field of engineering and bioscience. Interfacial rheology plays an important role in the dynamics of many of these systems, yet little is understood about how these effects alter droplet deformation and breakup. In this study, we develop a theoretical model that explores the deformation and breakup of a single droplet with a viscous surface modulus suspended in an unbounded immiscible fluid under a general linear flow field. The viscous interface is modeled as a two-dimensional surface having a surface shear viscosity η_μ , surface compression/dilational viscosity η_κ , and a constant surface tension over the interface, using a Boussinesq-Scriven constitutive relationship. We present the droplet breakup analysis in Stokes flow in the limit of small droplet deformation using a turning point analysis similar to that of Barthes-Biesel and Acrivos [*J. Fluid Mech.* **61**, 1 (1973)]. In particular, we examine how the critical capillary number for breakup depends on the interfacial viscosity for different viscosity contrasts between the inner and outer fluid and different flow types. For all the flows considered, we observe that η_κ is found to have a destabilizing impact on droplet breakup, whereas η_μ has a stabilizing effect. We explore the physical picture behind these observations in this work.

DOI: [10.1103/PhysRevFluids.5.063601](https://doi.org/10.1103/PhysRevFluids.5.063601)

I. INTRODUCTION

In recent years, understanding the dynamics of complex interfacial architectures between two immiscible fluids has gained the attention of many researchers. Membrane modifiers (for instance, surface-active agents or surfactants) are often added to emulsions to tailor them for applications in industry and bioscience. Polymer blends, vesicles, capsules, and lipid bilayers are some examples of fluid particles with complex interfaces, i.e., interfaces whose mechanics cannot be described solely by surface tension. From the modeling point of view, these complex fluid particles can be viewed as liquid droplets with a viscoelastic membrane of an adsorbed layer of surfactants, polymers, and proteins, to capture the mechanics of the system. Vesicles with membrane modifiers result in thin-shelled capsules [1–3]. These modified capsules are more robust and have greater colloidal stability, tunable membrane properties, and the ability to integrate a broad range of drugs and molecules. Polymersomes, another example of artificial vesicles, have been used to create controlled release drug delivery systems and have applications in medical imaging, electronics, and nanoreactors [1,3]. Given the diverse areas where one can find droplets with complex interfaces, it is important to understand how the rheology of such surfaces alters fundamental processes like

*vnarsim@purdue.edu

deformation, breakup, coalescence, and coarsening. By understanding the detailed dynamics of simpler processes (breakup, coalescence, deformation), one can develop quantitative guidelines on how to process multiphase fluids with a wide range of complicated, surface-active species. For example, the knowledge of deformation of an individual droplet can be employed to derive the effective stress of a dilute emulsion [4–6], and the knowledge of droplet breakup can help predict their dispersion performance in static mixers [7]. The correlations between single- and multiple-droplet phenomena (such as droplet breakup, coalescence, rising velocity, and axial dispersion) with droplet size and shape under different flow conditions can be used to develop kernels for population balance models [8–10].

In this paper, we will discuss droplet deformation and breakup. A single droplet placed in a viscous flow deforms as the external shear rate increases. For a sufficiently high shear rate, the viscous stresses on the surface are large enough to overcome the interfacial tension, and the droplet keeps deforming and ultimately breaks apart. Thus, there exists a maximum shear rate beyond which no stable droplet shape exists. Quantification of this breakup point can help predict the stability of emulsions as well as guide the design of multiphase flows in applications like printing, spraying, and blending.

There is extensive literature available on the deformation and breakup of a single clean droplet (with no surface-active agents on the interface) suspended in an immiscible fluid under an external flow. Barthes-Biesel and Acrivos [11] developed perturbation theories for predicting the conditions for the breakup of a droplet under a general linear flow field for small deformations. For large deformations, Hinch and Acrivos [12] analyzed long slender droplets in two-dimensional straining motion. Bentley and Leal [13] experimentally investigated the deformation of a droplet in a general flow field for both small and large deformations. Rallison [14] developed a numerical scheme to study the time-dependent deformation of a single viscous droplet in shear flow. Grace [7] predicted the dispersion performance of droplets in a static mixer with a high continuous phase viscosity through correlations of single-droplet deformation and breakup in extensional and shear flow fields. The diverse practical applications of droplet deformation and breakup in industry and bioscience were the motivation behind many of these earlier research problems. A wide range of prior work done on droplet deformation and burst is reviewed by Stone [15].

When surface-active agents are added to droplets, three primary effects occur: (1) lowering of surface tension, (2) inhomogeneous surfactant distribution on the droplet surface [16], and (3) change in interfacial rheology due to viscoelasticity of the membrane. The first two effects have been widely studied for simple surfactants in the context of droplet breakup [4,16–20]. The third effect, i.e., the impact of surface viscoelasticity, is less explored. For emulsions with more exotic surface-active and polymeric agents, the interface cannot be represented solely by surface tension effects, and interfacial viscosity and elasticity become essential. Surface shear and compressional viscosity and surface elasticity are the important parameters that control the interfacial behavior by introducing additional resistance to deformation from shearing and compression of the surface. These effects play an essential role in the stability of foams and emulsions [21]. There have been many experimental studies that measure the interfacial rheology of fluid-fluid surfaces using various types of instruments [22–24]. In the context of droplets, the studies on surface rheology focused on the deformation of a droplet with a purely elastic membrane. The deformation of elastic capsules in simple shear flow is reviewed in Barthès-Biesel [25]. Prior boundary element simulations of such systems are found in Li *et al.* [26] and experiments in Chang and Olbricht [27]. Little work has focused on purely viscous membranes or membranes with viscoelastic responses.

The presence of a concentrated monolayer of low-molecular-weight insoluble surfactants or polymers on the surface of a droplet can lead to a large degree of viscous dissipation on the interface due to high surface viscosity. This high surface viscosity is a result of the in-plane friction that arises when the molecular components on the interface slide past each other. Eicosanol (a fatty alcohol), hexadecanol (a low-molecular-weight surfactant), and the protein β -casein are some examples that form a predominantly viscous interface showing weak elastic behavior [24,28–30]. In an experimental study by Gunning *et al.* [30], the interface of β -casein-coated oil droplets showed

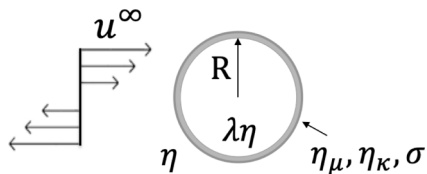


FIG. 1. Problem setup: dimensional quantities.

a fluidlike behavior when subjected to shear deformations. Erni [31] provides a review of the role that interfacial viscosity plays in the shear and dilational modes of deformation of complex fluid particles.

To our best knowledge, there is currently no analytical theory that quantifies the breakup of a surfactant-covered droplet with dominant surface viscous effects under a general linear flow field. Flumerfelt [32] adapted the previous perturbation analysis of Cox [33] on clean droplet deformation to include the effect of surface viscosities and examined the deformation and orientation of drops in shear and extensional flow fields. The limitation of this first-order perturbation analysis is that it cannot capture nonlinear rheology or breakup of droplets in shear flow. Recently Gounley *et al.* [34] developed numerical simulations to study the effect of surface viscosities on the deformation and stability of a single droplet suspended in an unbound shear flow. In this study, we will develop a theoretical model to understand the effect of interfacial viscosities on the stability of the droplet. The analytical model can capture droplet breakup behavior for a broad range of shear and dilational viscosities, under a wide range of flow types and viscosity ratios. We note that interfacial viscosity can significantly alter droplet deformation and breakup, which is consistent with observations by Phillips *et al.* [35].

II. METHOD OF ANALYSIS

A. Problem setup, goals, and underlying assumptions

Figure 1 shows a single droplet of radius R is suspended in an immiscible, unbound fluid. The viscosity of the fluid interior to the droplet is $\lambda\eta$ and exterior to the droplet is η . The droplet interface is embedded with a viscous insoluble monolayer of a surfactant or surface-active agent. This viscous monolayer is treated as a homogenous fluid obeying the Boussinesq-Scriven constitutive law [36,37] and has the following properties:

- (1) A constant surface shear viscosity η_μ
- (2) A constant surface dilational viscosity η_κ
- (3) Homogeneous surface tension, σ , and surfactant distribution over the surface.

The goal of this study is to examine how the presence of surface viscosities η_μ and η_κ impacts droplet breakup. The proposed theory neglects the inhomogeneity in surfactant concentration and surface tension, as well as interface elasticity. Surface concentration inhomogeneities can be neglected when either one of the following holds:

- (1) Surface diffusion of surfactant is much stronger than surface convection (i.e., $Pe_s = \frac{UR}{D_s} \ll 1$, where U is the velocity magnitude and D_s is the surface diffusivity of the species.)
- (2) Adsorption is stronger than surface convection and desorption, i.e., $Da_s = \frac{k_a c R}{U} \gg 1$ and $\frac{k_a c}{k_d} \gg 1$, where k_a and k_d are the kinetic constants for adsorption and desorption between the surface and bulk, and c is the concentration in the bulk.

When one of these conditions holds, Marangoni stresses can be incorporated into a modified surface dilational viscosity [38]. The effect of interfacial viscosities dominates over Marangoni effects when $\frac{MaPe_s}{Bq} = \frac{\Delta\sigma R^2}{\eta_s D_s} \ll 1$. In this expression, Ma is the Marangoni number, Bq is the shear or dilational Boussinesq number for surface viscosity η_s , Pe_s is the surface Péclet number, and $\Delta\sigma$ is the change in surface tension across the droplet. In reality, the above assumptions will hold

TABLE I. Dimensionless parameters.

| Parameter | Description | Formula | Typical range |
|-------------|---|---|-------------------------------|
| λ | Viscosity ratio | $\frac{\text{Inner fluid viscosity}}{\text{Outer fluid viscosity}}$ | $\lambda \sim O(1)–O(10)$ |
| Ca | Capillary number | $\frac{\eta\dot{\gamma}R}{\sigma}$ | $Ca \ll 1$ (0–0.25) |
| Bq_μ | Boussinesq parameter for surface shear viscosity | $Bq_\mu = \frac{\eta_\mu}{R\eta}$ | $Bq_\mu \sim O(0.1)–O(10)$ |
| Bq_κ | Boussinesq parameter for surface dilational viscosity | $Bq_\kappa = \frac{\eta_\kappa}{R\eta}$ | $Bq_\kappa \sim O(0.1)–O(10)$ |

for very small droplets (i.e., for nano- and micro-emulsions) or very strongly adsorbed surfactants [38,39]. When these assumptions do not hold, previous studies have shown that surface viscosities may vary strongly with surface pressure [29,40,41]. For now, we will isolate the effect that surface viscosities can play in droplet breakup and neglect the Marangoni contributions. We note that there is some experimental evidence that suggests that interfacial shear and dilational viscosity can have a significant impact on droplet deformation [35]. Another experimental study by Williams and Prins [42] discusses how interfacial shear and dilational rheology can impact breakup stability of droplets in the presence of a protein emulsifier (β -lactoglobulin and β -casein).

The droplet is subject to a general linear flow field expressed as $\tilde{u}_i^\infty = \tilde{\Gamma}_{ij}\tilde{x}_j$, where $\tilde{\Gamma}_{ij}$ is the far-field velocity gradient. $\dot{\gamma} = |\tilde{\Gamma}_{ij}|$ represents the characteristic magnitude of the far-field velocity gradient. We examine the problem in the zero Reynolds number limit ($Re = \rho\dot{\gamma}R^2/\eta$, where ρ is the outer fluid density). Thus the fluid motion inside and outside the droplet is governed by Stokes flow. We solve the Stokes flow inside and outside the droplet, subject to (a) continuity of velocity across the interface and (b) force balance at the interface. The latter condition corresponds to the tractions from surface tension and interfacial viscosities balancing the tractions from the external flow. The analysis presented is valid for small droplet deformation from its initial spherical shape, which is ensured by assuming a weak flow.

The Boussinesq-Scriven constitutive relationship and the associated boundary conditions for the problem setup are given in the Appendix.

B. Nondimensionalized parameters

All lengths are nondimensionalized by radius R of the initial spherical droplet, time by the capillary time scale $t_c = R\eta/\sigma$, viscosities by the outer fluid viscosity η , velocities by $R\dot{\gamma}$, stresses by $\eta\dot{\gamma}$, and surface stresses by $R\eta\dot{\gamma}$. Nondimensionalization of the problem leads to four critical dimensionless parameters. The dimensionless parameters are listed in Table I along with typical values explored in this study. The Bq_μ and Bq_κ range in Table I represents the practical values of these numbers found in some experimental studies [27,31,43,44]. For instance, for aqueous emulsion droplets embedded with different concentrations of PDMS-EO diblock copolymer surfactant, Bq_μ values are found to be very small ($Bq_\mu = 0.28–0.45$) as reported in an experimental study by Erk *et al.* [43]. Erni *et al.* [44] presented interfacial shear measurements for protein adsorbed onto oil-water and air-water droplet interfaces.

C. Droplet shape

In the limit of small deformation ($Ca \ll 1$), one can perform a regular perturbation expansion in capillary number Ca to solve for the flow field around the droplet to $O(Ca)$ and droplet shape to $O(Ca^2)$. Based on the symmetries of the droplet shape, the radius r_s of the deformed droplet is as

follows [45]:

$$r_s = 1 + \text{Ca} \frac{1}{r^2} D_{ij} x_i x_j + \text{Ca}^2 \left[-\frac{2}{15} D_{ij} D_{ij} + \frac{1}{r^4} D_{ijkl} x_i x_j x_k x_l \right] + O(\text{Ca}^3), \quad (1)$$

where $r = (x_l x_l)^{\frac{1}{2}}$ and x_i is the position vector on the droplet surface. All the position co-ordinates have been nondimensionalized by the radius R of the initial spherical drop. The first term in Eq. (1), i.e., $r_s = 1$, represents the equation of the surface of an undeformed drop. The second term is the $O(\text{Ca})$ ellipsoidal correction to droplet deformation. The third term gives the $O(\text{Ca}^2)$ correction that contains second and fourth-order harmonics. In Eq. (1), D_{lm} and D_{lmpq} are shape deformation tensors. As shown by Narsimhan [45], the differential equations for these tensors are

$$\begin{aligned} \frac{\partial D_{ij}}{\partial t} + \text{Ca}(D_{ik}\Omega_{kj} - \Omega_{ik}D_{kj}) \\ = a_E E_{ij} + a_D D_{ij} + \text{Ca} a_{DE} Sd_2[D_{ik}E_{kj}] + \text{Ca} a_{DD} Sd_2[D_{ik}D_{kj}] \\ + \text{Ca}^2 a_{E(D:D)} E_{ij}(D_{km}D_{km}) + \text{Ca}^2 a_{D(D:E)} D_{ij}(D_{km}E_{km}) \\ + \text{Ca}^2 a_{D(D:D)} D_{ij}(D_{km}D_{km}) + \text{Ca}^2 a_{EDD} Sd_2[E_{ik}D_{km}D_{mj}] \\ + \text{Ca}^2 a_{D4:E} D_{ijkl} E_{km} + \text{Ca}^2 a_{D4:D} D_{ijkl} D_{km} + O(\text{Ca}^3), \end{aligned} \quad (2)$$

$$\frac{\partial D_{ijkl}}{\partial t} = b_D D_{ijkl} + b_{DE} Sd_4[D_{ij}E_{kl}] + b_{DD} Sd_4[D_{ij}D_{kl}] + O(\text{Ca}). \quad (3)$$

In Eqs. (2) and (3), E_{ij} is the rate-of-strain tensor (symmetric part of velocity gradient) and Ω_{ij} is the vorticity tensor (antisymmetric part of velocity gradient):

$$\Gamma_{ij} = E_{ij} + \Omega_{ij}, \quad E_{ij} = \frac{1}{2}(\Gamma_{ij} + \Gamma_{ji}), \quad \Omega_{ij} = \frac{1}{2}(\Gamma_{ij} - \Gamma_{ji}).$$

The coefficients $[a_E, a_D, \dots]$ and $[b_D, b_{DE}, \dots]$ in Eqs. (2) and (3) are functions of the viscosity ratio λ and Bousinesq numbers Bq_μ and Bq_κ for the shear and dilational surface viscosities, respectively. The values of the coefficients are found in Narsimhan [45]. The terms Sd_2 and Sd_4 represent the symmetric, traceless portion of the second- and fourth-order tensors as follows:

$$\begin{aligned} Sd_2[A_{ij}] &= \frac{1}{2}(A_{ij} + A_{ji} - \frac{2}{3}A_{kk}\delta_{ij}), \\ Sd_4[A_{ij}B_{kl}] &= \frac{1}{6}(A_{ij}B_{kl} + A_{ik}B_{jl} + A_{il}B_{jk} + A_{jk}B_{il} + A_{jl}B_{ik} + A_{kl}B_{ij}) \\ &\quad - \frac{2}{21}Sd_2[A_{pm}B_{mq}](\delta_{ij}\delta_{kp}\delta_{ql} + \delta_{kl}\delta_{ip}\delta_{jq} + \delta_{ik}\delta_{jp}\delta_{lq} + \delta_{jl}\delta_{ip}\delta_{kq} + \delta_{il}\delta_{jp}\delta_{kq} + \delta_{jk}\delta_{ip}\delta_{lq}) \\ &\quad - \frac{2}{45}A_{mp}B_{mp}(\delta_{ij}\delta_{kl} + \delta_{ik}\delta_{jl} + \delta_{il}\delta_{jk}). \end{aligned}$$

An approach similar to Barthes-Biesel and Acrivos [11] and Vlahovska *et al.* [4] is adapted, and Eqs. (1), (2), and (3) are assumed to represent the droplet shape valid for $\text{Ca} \ll 1$. The steady-state solution to the droplet shape can be solved by setting the time derivatives to zero in Eqs. (2) and (3). Subsequent substitution of the expression for the fourth-order tensor, D_{ijkl} , from Eq. (3) into Eq. (2) results in the following steady-state equation for the second-order tensor D_{ij} :

$$\begin{aligned} -\text{Ca}(D_{ik}\Omega_{kj} - \Omega_{ik}D_{kj}) + a_E E_{ij} + a_D D_{ij} + \text{Ca} a_{DE} Sd_2[D_{ik}E_{kj}] + \text{Ca} a_{DD} Sd_2[D_{ik}D_{kj}] \\ + \text{Ca}^2 a_{E(D:D)} E_{ij}(D_{km}D_{km}) + \text{Ca}^2 a_{D(D:E)} D_{ij}(D_{km}E_{km}) + \text{Ca}^2 a_{D(D:D)} D_{ij}(D_{km}D_{km}) \\ + \text{Ca}^2 a_{EDD} Sd_2[E_{ik}D_{km}D_{mj}] - \text{Ca}^2 b_D^{-1} \{ (b_{DE} Sd_4[D_{ij}E_{km}] \\ + b_{DD} Sd_4[D_{ij}D_{km}]) (a_{D4:E} E_{km} + a_{D4:D} D_{km}) \} = 0. \end{aligned} \quad (4)$$

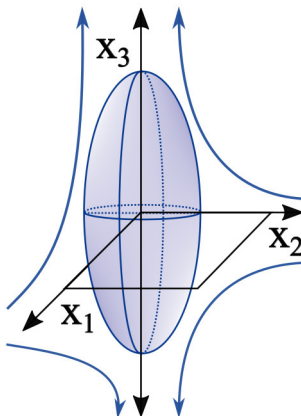


FIG. 2. Shape of a deformed droplet placed under uniaxial extensional flow.

D. Bifurcation analysis: $O(\text{Ca})$ and $O(\text{Ca}^2)$ theory

The steady-state equation (4) is cubic in D_{ij} and results in multiple solutions for the deformed droplet shape for a given set of external flow conditions and droplet material parameters. The steady-state analysis often results in a turning point bifurcation in the shape deformation tensor D_{ij} as the capillary number Ca is increased. Among the multiple solutions, only one is typically found to have a physically realistic droplet shape. In the $O(\text{Ca}^2)$ analysis presented here, we solve Eq. (4) up to $O(\text{Ca}^2)$ terms. For the $O(\text{Ca})$ analysis, higher-order terms are neglected and Eq. (4) is truncated to $O(\text{Ca})$ terms to provide the droplet shape solution.

The theory developed is valid for any general linear flow field. In this study, we analyze three canonical flow types: uniaxial extensional flow, planar extensional flow, and simple shear flow.

III. RESULTS: UNIAXIAL EXTENSIONAL FLOW

For uniaxial extensional flow, the external flow field in dimensionless form is represented as

$$u_1^\infty = -x_1, \quad u_2^\infty = -x_2, \quad u_3^\infty = 2x_3.$$

As shown in Fig. 2, the droplet gets compressed along the x_1 - x_2 plane and extended along the x_3 axis. The nondimensional rate-of-strain and vorticity tensors are, respectively:

$$E_{11} = E_{22} = -1, \quad E_{33} = 2 \quad \Omega_{ij} = 0.$$

Due to the axisymmetry of the flow and the form of velocity gradient tensor, it can be demonstrated that the solution to the steady-state shape deformation tensor D_{ij} in Eq. (4) takes a form similar to the velocity gradient:

$$D_{11} = D_{22} = D, \quad D_{33} = -2D.$$

Upon simplification, the steady-state equation reduces to a cubic in unknown D . D is solved for using the Newton-Raphson method in terms of Bq_μ , Bq_κ , Ca , and λ . A plot of D versus capillary number results in a turning point bifurcation curve for both the $O(\text{Ca})$ and $O(\text{Ca}^2)$ analyses (see Fig. 3). To navigate around the turning point, we start with the capillary number as the parameter in Newton's iterative solution method (i.e., we solve for D at a given Ca). Around the region where D changes sharply, we change the parameter to D (i.e., we solve for Ca at a given D). This technique is commonly used in the literature to analyze steady-state solutions around turning points [46–50]. One particular case of the bifurcation curve for $\lambda = 1$, $\text{Bq}_\mu = 0$, and $\text{Bq}_\kappa = 0$ is shown in Fig. 3. In this plot, positive values of capillary number correspond to extension along the x_3 axis and formation of

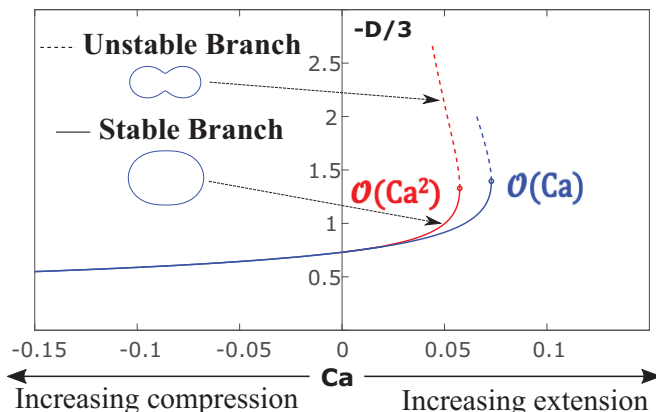


FIG. 3. Droplet deformation versus Ca in uniaxial flow, from both the $O(Ca)$ (blue line) and $O(Ca^2)$ (red line) analyses ($\lambda = 1$, $Bq_\mu = 0$ and $Bq_\kappa = 0$). The y axis is $-D/3$, where D is the x_1 component of the shape tensor D_{ij} . Positive values of Ca correspond to extension along the x_3 axis (prolate shape), and negative values of Ca correspond to compression along the x_3 axis (oblate shape). For this particular set of parameters, a droplet with $D < -2.2$ forms a prolate shape, while a droplet with $D > -2.2$ forms an oblate shape. The stable and unstable prolate droplet shapes at $Ca = 0.05$ are shown in the x_1 - x_3 plane.

prolate droplet shapes. Negative values of the capillary number correspond to compression along the x_3 axis and formation of oblate droplet shapes. As one marches along increasing capillary number, one goes from having one or two steady-state solutions to zero steady solutions. The capillary number at the turning point represents the critical capillary number Ca_C . If the flow rate is increased beyond Ca_C , the droplet will extend indefinitely and break apart, as there is no steady solution to the droplet shape. The critical capillary number separates the curves into two parts: a lower stable branch (bold lines) and an unstable upper branch (dashed lines that give unrealistic droplet shapes). The same observation was reported by Barthes-Biesel and Acrivos [11] for the clean droplet case. The $O(Ca^2)$ analysis of Barthes-Biesel and Acrivos [11] was found to be in better agreement with experimental results of Bentley and Leal [13]. The critical capillary number plots reported in this study make use of the $O(Ca^2)$ analysis unless otherwise noted.

A. Clean droplet

Figure 4 shows the dependence of the critical capillary number Ca_C on viscosity ratio λ for a clean droplet. We are exactly able to match the results with earlier breakup theories by Barthes-Biesel and Acrivos [11] and Vlahovska *et al.* [4]. The figure shows that the critical capillary number Ca_C decreases as the viscosity ratio λ increases. This implies that lower viscosity ratio droplets (for instance, air and vapor bubbles in water [$\lambda \sim (0-0.02)$]) would attain stable shapes even at elevated extension rates when compared to higher viscosity ratio drops like oil droplets in water [$\lambda \sim (10-100)$]. Small internal viscous resistance (i.e., $\lambda \ll 1$) seems to support highly elongated stable droplet shapes under flow. The reason for this observation is as follows: when a droplet is stretching under flow, a counterflow develops along the axis of stretching from the droplet pole towards the droplet center. When the pressure drop from this counterflow is larger than the original Laplace pressure of the droplet, i.e., $\Delta p > 2\sigma/R$, the droplet destabilizes. Since $\lambda \ll 1$ drops have small pressure gradients in the droplet interior, they are able to support larger droplet lengths before breakup. Note: a scaling analysis from Taylor for $\lambda \ll 1$ droplets shows that $Ca_C \sim \lambda^{-1/6}$ [53]. We note that the perturbation theory discussed in this paper fails to provide accurate predictions for droplet deformation and breakup for $\lambda \ll 1$ as the droplet is too elongated, and hence is no longer in the small deformation regime. The theory discussed here is valid for $\lambda \sim O(1)$.

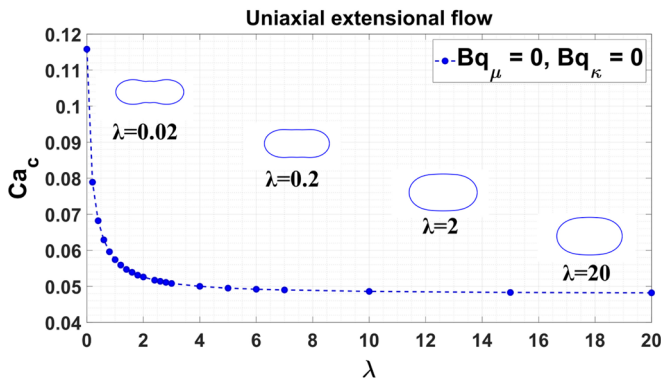


FIG. 4. Ca_C versus λ for a clean droplet in uniaxial extensional flow. The snapshots are deformed droplet shapes at Ca_C . Note: for $\lambda = 0.02$, the shape from the perturbation analysis is not valid because the droplet is highly deformed. Slender body droplet theories like in Refs. [12,51,52] are more valid in this regime ($\lambda \ll 1$).

In Secs. III B and III C we see how the presence of surface viscosities (dilational and shear) alters the dependence of Ca_C on λ .

B. Effect of surface dilational viscosity: η_κ

The isolated effect of surface dilational viscosity on droplet stability can be examined through tuning the dilational Boussinesq number Bq_κ . Figure 5(a) shows the dependence of Ca_C on viscosity ratio λ for different values of Bq_κ . Upon increasing Bq_κ , the Ca_C decreases and the droplet breaks at a relatively lower capillary number compared to a clean droplet. This does not represent an intuitive result as one would expect an increase in dilational resistance to make droplet breakup more difficult. The reduced stability limit here can be attributed to the enhanced deformation of the droplet when surface dilational resistance is present at a given capillary number and viscosity ratio. Figure 5(b) shows a schematic of the mechanism. When a droplet stretches in flow, there is dilation at the droplet's equator and compression at the droplet's pole. If dilational resistance is

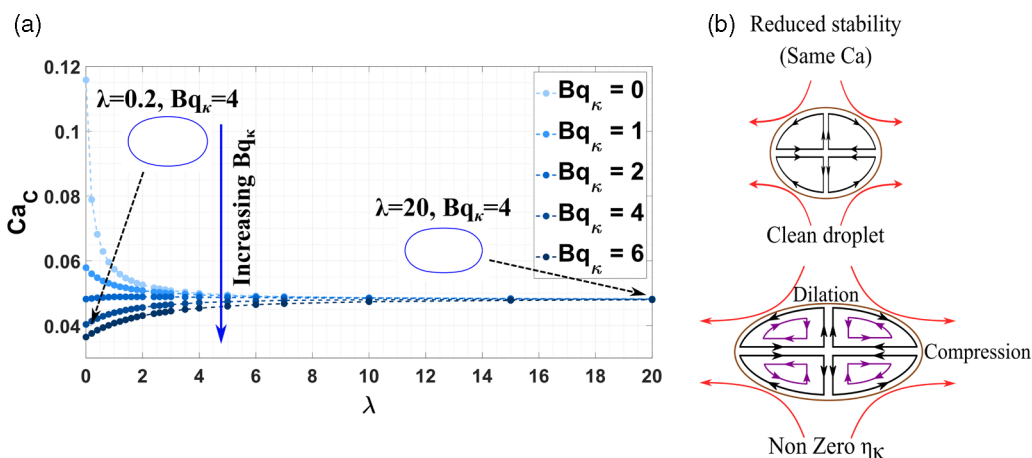


FIG. 5. (a) Ca_C versus λ for different dilational Boussinesq numbers Bq_κ in uniaxial extensional flow. The shear Boussinesq number $Bq_\mu = 0$. The snapshots are at Ca_C . (b) Schematic of the mechanism behind reduced stability. Black lines represent the existing circulation pattern, and purple lines are the induced counterflow from interfacial effects.

present, the compression pattern at the surface induces a counterflow that results in reduced fluid circulation inside the droplet. This reduced circulation increases droplet deformation compared to a clean droplet at the same capillary number and viscosity ratio.

Another way to think of the mechanism is to examine the Boussinesq-Scriven equation for interfacial stresses [Eq. (5)]:

$$\mathbf{f} = -2 \frac{H}{Ca} \mathbf{n} + Bq_k \nabla_s \cdot (\Theta \mathbf{P}). \quad (5)$$

In the above equation, \mathbf{f} is the traction on the surface in dimensionless form. \mathbf{n} is the outward-pointing normal vector, H is the mean curvature, and Θ is the surface rate of dilation. \mathbf{P} is the projection operator on the surface, and ∇_s is the surface gradient. In regions where the dilation rate is negative (e.g., compression occurs), the capillary forces counteract the compressional resistance by increasing surface curvature. This outcome leads to enhanced elongation at the droplet poles, which assists droplet stretching and lowers the critical capillary number.

We note that surface dilational viscosity appears to have a similar effect as surfactant convection on droplet stability [19,54]. During surface convection, the surfactant is swept towards the droplet pole, which reduces the surface tension at the pole. In order to balance the external viscous forces at this location, the droplet elongates, leading to enhanced deformation and a lowering of Ca_C . Surface convection also leads to a reduction in internal circulation like in Fig. 5(b).

We find that for viscosity ratios $\lambda \sim O(1)$, the dilational viscosity can have a significant impact on droplet breakup ($\sim 29\%$ lowering of Ca_C when Bq_k goes from 0 to 6). However, when the viscosity ratio becomes very large ($\lambda \gg 1$), a droplet with surface dilational viscosity essentially behaves the same as a clean droplet, i.e., any further increase in surface dilational viscosity has no significant impact on the critical capillary number. The reason for the observation is as follows. At large values of the viscosity ratio, the viscous tractions from the flow field dominate the dilational tractions on the droplet due to surface viscosity. When the fluid inside the droplet is highly viscous ($\lambda > 10$), the viscous dissipation in the droplet interior does not lead to significant deformation upon increasing Ca . All droplets with $\lambda > 10$ break roughly at the same Ca_C .

C. Effect of surface shear viscosity: η_μ

Surface shear viscosity is found to have a stabilizing impact on droplet breakup. Upon increasing the shear Boussinesq number Bq_μ , the droplet breaks up at a larger capillary number compared to a clean droplet at the same viscosity ratio λ [Fig. 6(a)]. The reason for the enhanced stability limit of a droplet with surface shear viscosity can be attributed to its reduced deformation compared to a clean droplet at a given capillary number and viscosity ratio [Fig. 6(b)]. Let us examine the Boussinesq-Scriven equation for interfacial stresses [Eq. (6)]:

$$\mathbf{f} = -2 \frac{H}{Ca} \mathbf{n} - Bq_\mu \nabla_s \cdot (\Theta \mathbf{P} - 2 \mathbf{e}_s). \quad (6)$$

In the above equation, \mathbf{e}_s is the surface rate of the strain tensor.

There are two mechanisms that show the effect of surface shear viscosity on droplet deformation. First, the formula shows that surface shear viscosity has the opposite effect on dilation rate compared to surface dilational viscosity. Because of this effect, the curvature at the poles of the droplet will decrease to counteract the compression in these regions. This outcome reduces droplet deformation and increases the critical capillary number. The second mechanism involves the surface rate of the strain tensor. The viscous dissipation on the surface due to surface shear viscosity can be related to \mathbf{e}_s using the formulation developed by Secomb and Skalak [55]. As the surface shear viscosity increases, the viscous dissipation on the interface also increases. This viscous dissipation tends to reduce the surface rate of deformation on the droplet and further stabilizes the droplet.

We note that surface shear viscosity appears to have a similar effect on droplet stability as surfactant dilution, in that both increase the critical capillary number compared to a clean droplet. During surfactant dilution, the dilation of a droplet surface under flow leads to the distribution of

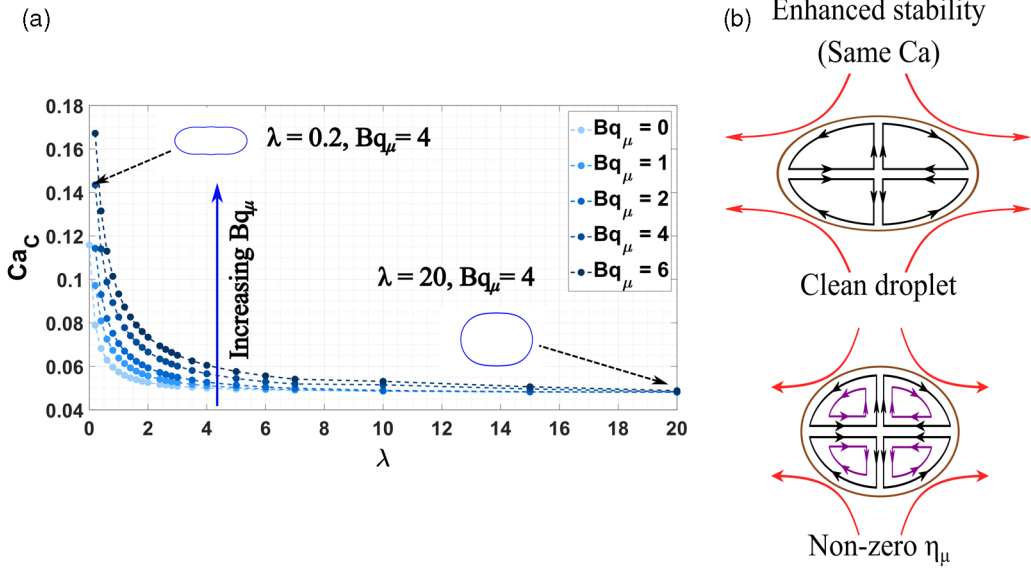


FIG. 6. (a) Ca_C versus λ for different shear Boussinesq numbers Bq_μ in uniaxial extensional flow. The dilational Boussinesq number $Bq_\kappa = 0$. The snapshots are at Ca_C . (b) Schematic of the mechanism behind enhanced stability. Black lines represent the existing circulation pattern, and purple lines are the induced flow from interfacial effects.

surfactant across an increased interfacial area. The diluted surfactant concentration stabilizes the droplet by increasing the surface tension of the interface compared to its value for the undeformed shape. This effect leads to reduced deformation of the droplet when compared to a clean droplet at the same flow rate and viscosity ratio [19,54].

For very high values of viscosity ratio ($\lambda > 10$), it can be noted that surface shear viscosity has negligible impact on Ca_C [Fig. 6(a)].

D. Effect of equal surface viscosity: $Bq_\mu = Bq_\kappa = Bq$

The theory developed here can be used to predict Ca_C for any general combinations of Bq_μ , Bq_κ , and λ . Figure 7 shows one particular case where the interface has equal surface shear and

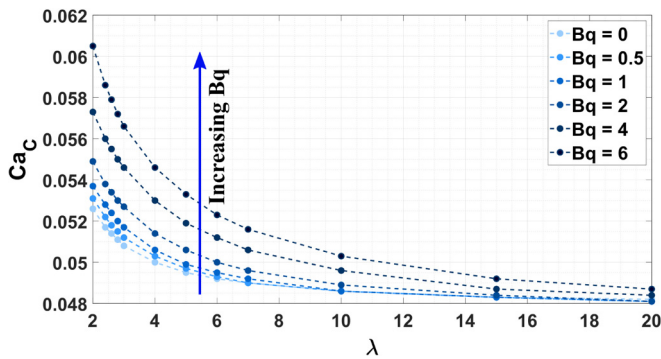


FIG. 7. Ca_C versus λ at different values of $Bq_\mu = Bq_\kappa = Bq$ under uniaxial flow. $Bq = 0$ corresponds to a clean droplet.

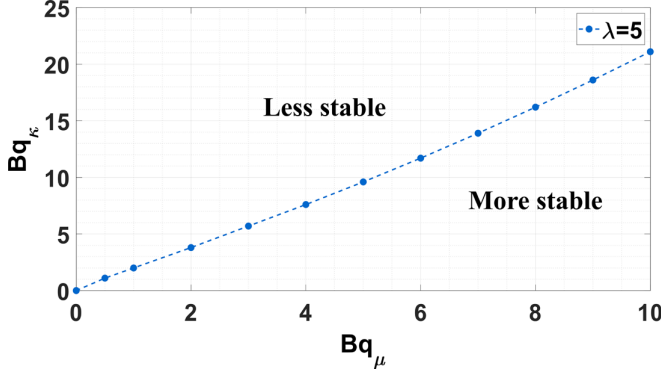


FIG. 8. Combination of Boussinesq numbers that have a Ca_C identical to that of a clean droplet under uniaxial flow at $\lambda = 5$. “Less stable” (“more stable”) implies that the droplet has its critical point at a lower (higher) Ca_C than a clean droplet at the same viscosity ratio.

dilational viscosities, for viscosity ratio $\lambda \geq 2$. From the plot, it can be noted that the overall impact of equal surface viscosities is to increase Ca_C from that of clean droplet even for small values of $Bq = Bq_\mu = Bq_\kappa$. For a droplet with equal surface viscosities, the Boussinesq-Scriven equation for interfacial stresses reduces to Eq. (7):

$$\mathbf{f} = -2\frac{H}{Ca}\mathbf{n} + Bq\nabla_s \cdot 2\mathbf{e}_s. \quad (7)$$

From Eq. (7) we see that the rate of dilation does not appear in the interfacial stress balance and only the $Bq\nabla_s \cdot 2\mathbf{e}_s$ term exists. This leads to viscous dissipation on the interface, which increases upon increasing Bq . The viscous dissipation due to the presence of finite Bq reduces the surface rate of the deformation of the droplet and stabilizes the droplet. Similar observations have been reported in previous studies examining the effect of equal surface viscosities [34,56].

For some combinations of Bq_μ and Bq_κ (represented by the curve in Fig. 8 for one particular case of $\lambda = 5$), the critical capillary values are found to be the identical as that of a clean droplet at the same viscosity ratio. In Fig. 8 all the combinations of Bq_κ and Bq_μ below the curve would break at a larger Ca_C than a clean droplet, and all combinations above the curve would break at a lower Ca_C than a clean droplet.

IV. RESULTS: HYPERBOLIC FLOW

For a planar hyperbolic flow, the undisturbed external flow field in dimensionless form is

$$u_1^\infty = x_1, \quad u_2^\infty = -x_2, \quad u_3^\infty = 0.$$

The nondimensional rate-of-strain and vorticity tensors are

$$E_{11} = -E_{22} = 1, \quad \Omega_{ij} = 0.$$

Figure 9 shows that x_1 is the axis along which the droplet gets extended, and x_2 is the axis of compression. Again, from the symmetry of the external flow field, the steady-state solution of the shape tensor D_{ij} in Eq. (4) will be of the form

$$D_{11} = D_1, \quad D_{22} = D_2, \quad D_{33} = -(D_1 + D_2).$$

Upon simplification, the steady-state equation reduces to two coupled nonlinear equations in unknowns D_1 and D_2 . The system of equations for D_1 and D_2 can be solved using the Newton-Raphson method for a given value of viscosity ratio λ and Boussinesq surface viscosity parameters Bq_μ and Bq_κ . The plot of either component of the shape deformation tensor (D_1 or D_2) versus

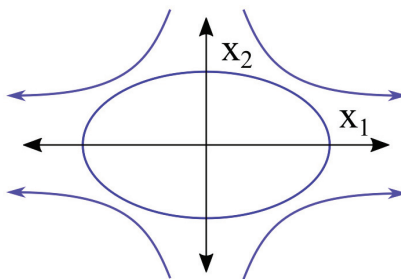


FIG. 9. Deformed droplet shape in planar hyperbolic flow.

capillary number results in a turning point bifurcation curve for both the $O(\text{Ca})$ and $O(\text{Ca}^2)$ analyses. One particular case of $\lambda = 1$, $\text{Bq}_\mu = 2$, and $\text{Bq}_\kappa = 2$ is shown in Fig. 10. The capillary number at the turning point is the critical value Ca_C beyond which there exists no stable solution to the droplet shape. In the following sections, we will discuss the dependence of this critical capillary number Ca_C on the viscosity ratio for a clean droplet and a droplet with surface viscosity.

A. Clean droplet

Similar to uniaxial extensional flow, the critical capillary number Ca_C decreases with an increase in viscosity ratio λ for a droplet with no surfactant on the surface. The lower viscosity ratio droplets are found to be more elongated around the critical point compared to droplets with a higher viscosity ratio. The dependence of Ca_C on viscosity ratio is plotted in Fig. 11 along with experimental results from Bentley and Leal [13]. The Ca_C values reported are from the $O(\text{Ca}^2)$ analysis. As can be seen from Fig. 11, the theoretical results match well with the experimental results for all viscosity ratios except very low λ ($\lambda < 0.2$). For $\lambda \ll 1$, there is a discrepancy between the two results. The theory fails in this region as the droplet forms highly elongated shapes, and the small deformation assumption is no longer valid.

B. Effect of surface shear viscosity η_μ and surface dilational viscosity η_κ

The isolated effect of surface shear viscosity and dilational viscosity on droplet breakup is similar to what was observed for uniaxial extensional flow. Figures 12 and 13 show the dependence of Ca_C on viscosity ratio for different surface shear and dilational Boussinesq numbers. We observe that

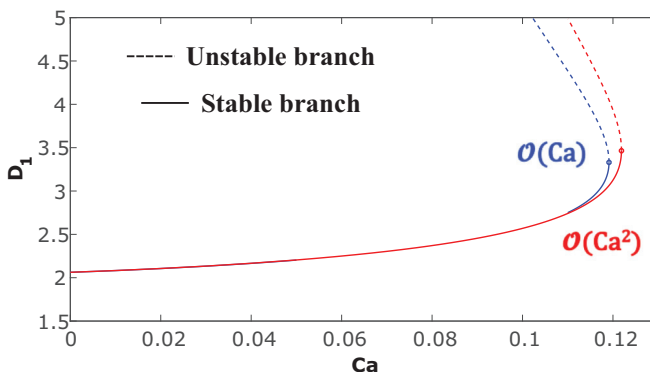


FIG. 10. D_1 (x_1 component of shape tensor) versus Ca from both $O(\text{Ca})$ (blue lines) and $O(\text{Ca}^2)$ (red lines) analyses for planar hyperbolic flow. Lower branches (bold lines) represent stable solutions, and the upper branches represent unstable states.

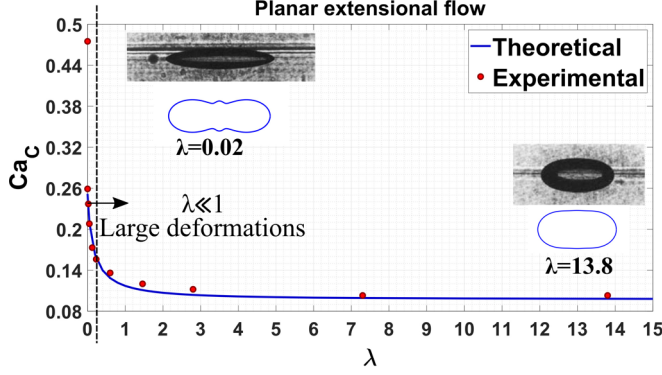


FIG. 11. Comparison between theoretical and experimental values of Ca_C , for a clean droplet ($Bq_\mu = Bq_\kappa = 0$) in planar hyperbolic flow. Experimental results are from Bentley and Leal [13]. The theory does not provide accurate predictions for $\lambda \ll 1$ (demarcated by vertical dotted line), as deformations are large.

surface shear viscosity has a stabilizing effect on droplet breakup (i.e., it increases Ca_C compared to a clean droplet at the same viscosity ratio), while surface dilational viscosity has a destabilizing effect. The critical capillary numbers for planar extensional flow are higher than that for uniaxial extensional flow. The mechanism behind enhanced and reduced stability for the two cases is similar to what was discussed for uniaxial extensional flow.

V. RESULTS: SIMPLE SHEAR FLOW

For a simple shear flow, the undisturbed external flow field in the dimensionless form is

$$u_1^\infty = 2x_2.$$

This flow can be seen as a combination of extension and rotation (Fig. 14). The nondimensional rate-of-strain and vorticity tensors are

$$E_{12} = E_{21} = 1, \quad \Omega_{12} = -\Omega_{21} = 1.$$

Unlike extensional flow, a simple shear flow exhibits nonzero vorticity effects. Based on the form of the external velocity gradient, the solution to the steady-state equation will be of the form

$$D_{11} = D_1, \quad D_{22} = D_2, \quad D_{33} = -(D_1 + D_2), \quad D_{12} = D_3.$$

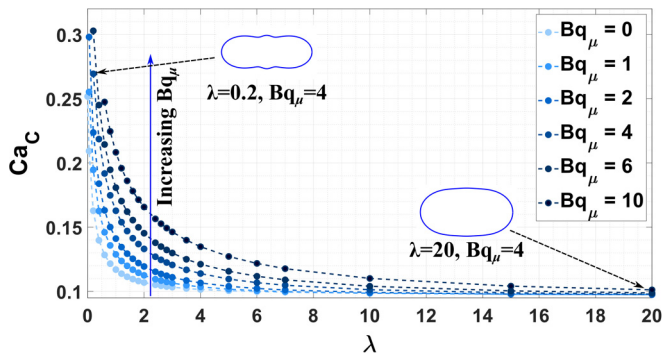


FIG. 12. Ca_C versus λ at different values of Bq_μ in planar hyperbolic flow. The dilational Boussinesq number is $Bq_\kappa = 0$. The snapshots are at Ca_C .

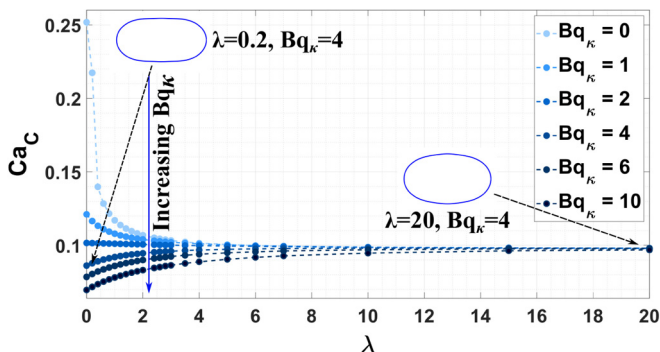


FIG. 13. Ca_C versus λ at different values of Bq_κ in planar hyperbolic flow. The shear Boussinesq number is $Bq_\mu = 0$. The snapshots are at Ca_C .

Upon simplification, the steady-state equation reduces to three coupled nonlinear equations for unknowns D_1, D_2 , and D_3 . The system of equations is solved using the Newton-Raphson method.

In the $O(Ca)$ analysis for simple shear flow, where the $O(Ca^2)$ terms in the steady-state equation [Eq. (4)] are neglected, no bifurcation curves are observed. Stable droplet shapes are instead found for all small perturbations, which is not observed experimentally for clean droplets. Therefore, no breakup information can be obtained using the $O(Ca)$ analysis in case of shear flow. We will discuss results for the $O(Ca^2)$ analysis below.

A. Clean droplet

In shear flow, the dependence of Ca_C on viscosity ratio λ is quite different from what was observed in uniaxial extensional flow and planar hyperbolic flow. Results are shown in Fig. 15 along with experimental data from Torza *et al.* [57]. Unlike hyperbolic flow, the experimental results for shear flow do not match the theory particularly well. This is generally the case for perturbation theories since the critical capillary numbers for experiments in shear flow ($Ca > 0.25$) are often larger than the values in which the theories are strictly valid (i.e., $Ca \ll 1$). Nevertheless, the theories capture the qualitative trends in droplet breakup reasonably well.

In shear flow, our theory observes only stable shapes, and hence no critical capillary number, for droplets at a low-viscosity ratio ($\lambda < 0.14$) and high-viscosity ratio ($\lambda > 2.8$). This result is consistent with Barthes-Biesel and Acrivos [11]. In actuality, a critical Ca_C does exist experimentally in these regions, but they are very large ($Ca_C \gg 1$) and hence fall outside the range of validity of our theory. For intermediate viscosity ratios ($0.14 < \lambda < 2.8$), our theory predicts a critical capillary number Ca_C of $O(1)$ or below. The reason why low-viscosity ratio ($\lambda \ll 1$) droplets have a very large Ca_C is the same as discussed earlier for extensional flow—steady high elongation of the droplet is achievable when the droplet interior has small viscous resistance. For very high-viscosity ratios ($\lambda \gg 1$), the droplet rotates towards the flow axis due to nonzero vorticity. It does not deform much on increasing the flow rate, essentially behaving as a rigid body. Figure 15 shows images from

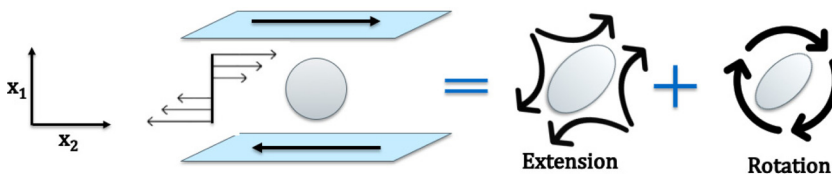


FIG. 14. Droplet placed under simple shear flow.

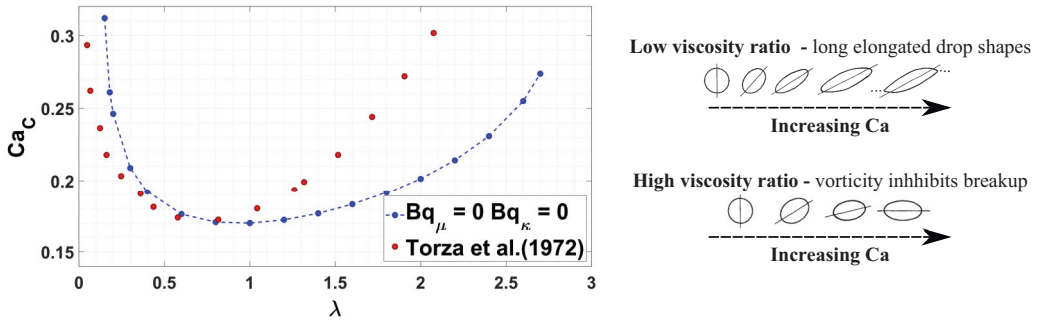


FIG. 15. Ca_C versus λ for a clean droplet (i.e., $Bq_\mu = Bq_\kappa = 0$) in shear flow along with experimental results from Torza *et al.* [57]. Experimental images on the right are from Rumscheidt and Mason [58]. These images represent how a droplet's shape will change as Ca increases for a low-viscosity ratio droplet ($\lambda = 2 \times 10^{-4}$) and a high-viscosity ratio droplet ($\lambda = 6$). At large Ca , a low-viscosity ratio droplet forms pointed ends from which small droplets eject (as depicted by the dashed lines emanating from the droplet tips).

an experimental study on clean droplet breakup by Rumscheidt and Mason [58]. These images represent how a droplet's shape will change as the capillary number increases for a low-viscosity ratio droplet ($\lambda = 2 \times 10^{-4}$) and a high-viscosity ratio droplet ($\lambda = 6$).

B. Effect of surface shear viscosity η_μ and surface dilational viscosity η_κ

Just like in uniaxial extensional flow and planar hyperbolic flow, we observe surface shear viscosity to be stabilizing—in other words, a droplet with finite Bq_μ has a higher Ca_C than a clean droplet at the same viscosity ratio. The effect of surface dilational viscosity has the opposite effect—it lowers Ca_C compared to a clean droplet. The mechanisms behind the enhanced and reduced stability limits are similar to what we discussed previously.

Figures 16 and 17 show the dependence of Ca_C on viscosity ratio in shear flow for increasing values of Bq_μ and Bq_κ . Upon increasing the surface dilational viscosity, the range of λ for which Ca_C is observed becomes larger, while upon increasing surface shear viscosity, the range gets smaller. The figures also show some snapshots of droplet deformation at the critical point. We note that some droplet shapes in shear flow have bumps in the equator region (Fig. 16), which was also observed in other perturbation theories by Barthes-Biesel and Acrivos [11] and Vlahovska *et al.* [4].

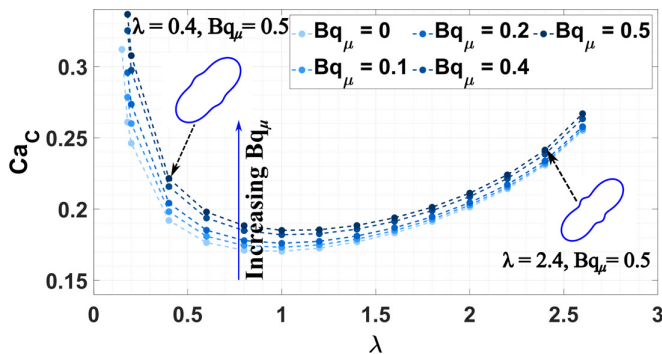


FIG. 16. Ca_C versus λ at different values of Bq_μ in shear flow. The dilational Boussinesq number is $Bq_\kappa = 0$. The snapshots are shown at Ca_C .

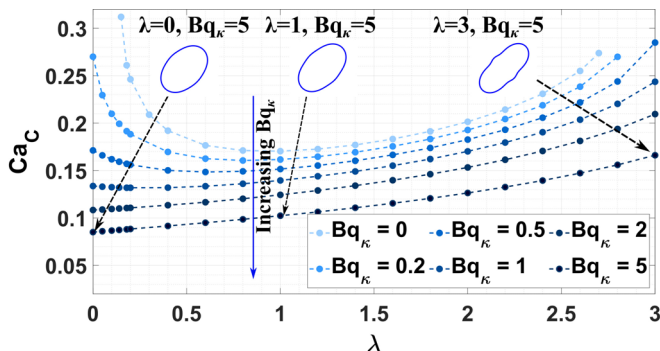


FIG. 17. Ca_C versus λ at different values of Bq_κ in shear flow. The shear Boussinesq number is $Bq_\mu = 0$. The snapshots are shown at Ca_C .

As discussed by Barthes-Biesel and Acrivos [11], these bumps will not be observed experimentally but can be likely resolved through higher order perturbation theories.

One interesting observation from our theories is that not only does dilational viscosity reduce the Ca_C of a droplet at a given viscosity ratio, but it appears to reduce the deformation at breakup as well. This point is evident in Fig. 17, where a clean droplet at $\lambda \ll 1$ is known to be highly elongated at its critical point, but appears to be a mildly deformed spheroid at its critical point when $Bq_\kappa = 5$. Although this observation will have to be verified by experiments or simulations, it suggests that small deformation theories may be reasonable in predicting droplet shapes near critical points for bubbles with large values of Bq_κ , where such theories would otherwise fail for clean droplets. We note that increasing Bq_κ to a sufficiently high value ($Bq_\kappa \gtrsim 0.4$) results in the breakup of very low- and very high-viscosity ratio droplets, which otherwise would have been stable in clean droplets under small perturbations (Fig. 17).

Figure 18 plots the combinations of Boussinesq numbers that yield the same critical capillary number as that of a clean droplet at viscosity ratio $\lambda = 1$. Boussinesq numbers above the curve imply that breakup will happen at a Ca_C lower than that of a clean droplet (coined “less stable”), while data below the curve imply that breakup will happen at a Ca_C higher than that of a clean droplet (coined “more stable”). As can be noted from Fig. 18, at each point on the curve for $Bq_\mu > 0.5$,

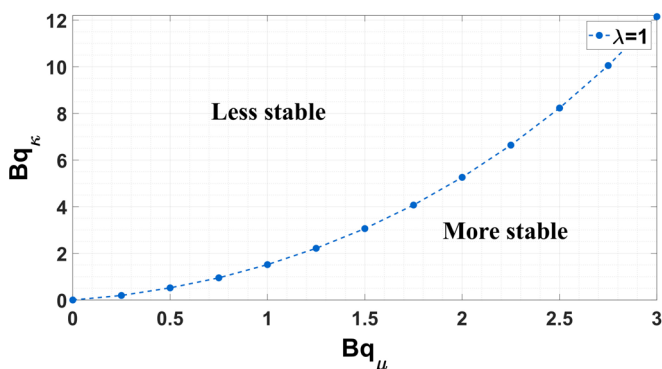


FIG. 18. Combination of Boussinesq numbers that have a Ca_C identical to that of a clean droplet under shear flow at $\lambda = 1$. “Less stable” (“more stable”) implies that the droplet has its critical point at a lower (higher) Ca_C than a clean droplet at the same viscosity ratio.

$Bq_\kappa/Bq_\mu \geq 1$. This suggests that the stabilizing effect of surface shear viscosity dominates the destabilizing effect of surface dilational viscosity, just like in uniaxial and planar hyperbolic flows.

For $\lambda = 0.5$, increasing Bq_μ from 0 to 1 results in roughly a 26% increase in the critical capillary number (Fig. 16). For the same viscosity ratio, increasing Bq_κ from 0 to 1 drops the critical capillary number by roughly 27% (Fig. 17). From the above, it appears that surface viscosities could have a significant impact on droplet stability.

VI. CONCLUSION

In this study, we present conditions for the breakup of a droplet with viscous surface moduli, under the assumption of weak flow and negligible Marangoni forces. The viscous droplet interface is modeled by the linear Boussinesq-Scriven constitutive relationship. Using the small deformation perturbation theories developed by Narsimhan [45], we analyze the critical conditions leading to the breakup of the droplet under different flow types. For the three flows presented (uniaxial extensional, planar hyperbolic, and simple shear flow), we observed that surface shear viscosity η_μ increases the critical capillary number at a given viscosity ratio (i.e., stabilizes the droplet), while dilational surface viscosity η_κ lowers the critical capillary number at a given viscosity ratio (i.e., destabilizes the droplet).

For the clean droplet results presented here, we are able to precisely match the critical capillary number with earlier small deformation theories (Barthes-Biesel and Acrivos [11] and Vlahovska *et al.* [4]). The validity of the small deformation theories with numerical studies in shear and extensional flow is reviewed in Acrivos [59] and Rallison [60]. In general, the numerical results of Rallison and Acrivos [61] and Rallison [14] are found to be in good qualitative agreement with the small deformation theories for a wide range of viscosity ratios, except when $\lambda \ll 1$ where slender body theories work well [12,51,52]. The critical capillary numbers from analytic theories are found to be within 15% of the numerical results for extensional flow and within 20% for shear flow. For example, at viscosity ratio $\lambda = 1$, the critical capillary number in shear flow from analytic theories is $Ca_c = 0.34$, whereas results from several numerical studies lie in the range $0.34 < Ca_c < 0.43$. [5,14,34,62–65]. For a clean droplet, the $O(Ca^2)$ analyses of earlier small perturbation theories [11] are found to be in better agreement with experiments [13].

When surface viscosity is present on a droplet, the dependence of Ca_c on λ is qualitatively similar to that of a clean droplet. At a given viscosity ratio, the isolated impact of surface shear viscosity is to increase the Ca_c , while dilational viscosity is to decrease the Ca_c . The destabilizing effect of surface dilational viscosity appears similar to surfactant convection effects, while the stabilizing impact of surface shear viscosity appears similar to surfactant dilution. One particularly intriguing observation in the case of extensional flows is that increasing the surface viscosities after a specific value of viscosity ratio ($\lambda \approx 20$) has no significant impact on Ca_c . The surfactant-covered droplet essentially behaves the same as a clean droplet.

Validation of the deformation and breakup theories presented here will require an experimental investigation of the deformation of a single, small droplet with viscous interfacial rheology or numerical simulations that investigate similar phenomena. In particular, it would be useful to know the accuracy of the $O(Ca)$ or $O(Ca^2)$ analyses presented here. We note that some surface-active species that can show predominantly viscous behavior include eicosanol (a fatty alcohol), hexadecanol (a low-molecular-weight surfactant), or the protein β -casein [24,28–30]. In this analysis, we neglect the inhomogeneous distribution of surfactant and interfacial elasticity effects. Even with these assumptions relaxed, we believe that the qualitative trends of surface viscosity will remain the same, i.e., η_κ is destabilizing whereas η_μ is stabilizing, as similar observations have been reported in a recent numerical study by Luo *et al.* [62] that examines the effect of equal surface viscosities on surfactant transport. They report that the surface shear viscosity inhibits local convection, while the surface dilational viscosity inhibits local dilution.

ACKNOWLEDGMENT

The authors would like to acknowledge the input from the anonymous reviewers, which greatly improved this paper.

APPENDIX: GOVERNING EQUATIONS

For a droplet subject to a linear flow field, the fluid motion inside and outside the droplet is governed by the Stokes equations. In dimensionless form, these equations are

$$\lambda \nabla^2 \mathbf{u}^{\text{in}} = \nabla p^{\text{in}}, \quad \nabla \cdot \mathbf{u}^{\text{in}} = 0,$$

$$\nabla^2 \mathbf{u}^{\text{out}} = \nabla p^{\text{out}}, \quad \nabla \cdot \mathbf{u}^{\text{out}} = 0.$$

The boundary conditions are the following:

- (1) Continuity of velocity at the interface

$$\mathbf{u}^{\text{in}} = \mathbf{u}^{\text{out}}$$

- (2) Force balance at interface

$$(\boldsymbol{\sigma}^{\text{in}} - \boldsymbol{\sigma}^{\text{out}}) \cdot \mathbf{n} = \mathbf{f}$$

- (3) Kinematic boundary condition

$$\frac{D}{Dt}[r - r_s(\theta, \phi, t)] = 0.$$

In the force-balance, the traction \mathbf{f} due to interfacial stresses is

$$\mathbf{f} = -2 \frac{H}{\text{Ca}} \mathbf{n} + (\text{Bq}_\kappa - \text{Bq}_\mu) \nabla_s \cdot (\Theta \mathbf{P}) + \text{Bq}_\mu \nabla_s \cdot (2 \mathbf{e}_s),$$

where \mathbf{n} is the outward-pointing normal vector, $H = \frac{1}{2} (\nabla_s \cdot \mathbf{n})$ is the mean curvature, Bq_μ is the Boussinesq number for surface shear viscosity, Bq_κ is the Boussinesq number for surface dilational viscosity, Θ is the surface rate of dilation, and \mathbf{e}_s is the surface rate of strain tensor. $\mathbf{P} = \mathbf{I} - \mathbf{nn}$ is projection operator on the surface, and $\nabla_s = \mathbf{P} \cdot \nabla$ is the surface gradient. The following are the definitions for the surface rate of strain tensor \mathbf{e}_s and the surface rate of dilation Θ :

$$\mathbf{e}_s = \frac{1}{2} \mathbf{P} \cdot [\nabla_s \mathbf{u}^s + (\nabla_s \mathbf{u}^s)^T] \cdot \mathbf{P}, \quad \Theta = \mathbf{P} : \nabla_s \mathbf{u}^s.$$

In the above expression, \mathbf{u}^s is the velocity at the droplet surface. In the kinematic boundary condition, $r_s(\theta, \phi, t)$ is the shape of the droplet described by Eq. (1) in the limit $\text{Ca} \ll 1$. $\frac{D}{Dt} = (\frac{1}{\text{Ca}} \frac{\partial}{\partial t} + u_i \frac{\partial}{\partial x_i})$ is the substantial derivative in nondimensional form.

-
- [1] J. S. Lee and J. Feijen, Polymersomes for drug delivery: Design, formation and characterization, *J. Controlled Release* **161**, 473 (2012).
- [2] D. Barthes-Biesel, Motion and deformation of elastic capsules and vesicles in flow, *Annu. Rev. Fluid Mech.* **48**, 25 (2016).
- [3] B. M. Discher, Y.-Y. Won, D. S. Ege, J. C. Lee, F. S. Bates, D. E. Discher, and D. A. Hammer, Polymersomes: Tough vesicles made from diblock copolymers, *Science* **284**, 1143 (1999).
- [4] P. M. Vlahovska, J. Bławdziewicz, and M. Loewenberg, Small-deformation theory for a surfactant-covered drop in linear flows, *J. Fluid Mech.* **624**, 293 (2009).
- [5] M. Kennedy, C. Pozrikidis, and R. Skalak, Motion and deformation of liquid drops, and the rheology of dilute emulsions in simple shear flow, *Comput. Fluids* **23**, 251 (1994).

- [6] N. Frankel and A. Acrivos, The constitutive equation for a dilute emulsion, *J. Fluid Mech.* **44**, 65 (1970).
- [7] H. P. Grace, Dispersion phenomena in high viscosity immiscible fluid systems and application of static mixers as dispersion devices in such systems, *Chem. Eng. Commun.* **14**, 225 (1982).
- [8] G. Narsimhan, Z. Wang, and N. Xiang, Guidelines for processing emulsion-based foods, *Food Emulsifiers and Their Applications* (Springer, New York, 2019), pp. 435–501.
- [9] M. Simon, S. A. Schmidt, and H.-J. Bart, The droplet population balance model—estimation of breakage and coalescence, *Chem. Eng. Technol.* **26**, 745 (2003).
- [10] B. Sajjadi, A. A. A. Raman, R. S. S. R. E. Shah, and S. Ibrahim, Review on applicable breakup/coalescence models in turbulent liquid-liquid flows, *Rev. Chem. Eng.* **29**, 131 (2013).
- [11] D. Barthes-Biesel and A. Acrivos, Deformation and burst of a liquid droplet freely suspended in a linear shear field, *J. Fluid Mech.* **61**, 1 (1973).
- [12] E. Hinch and A. Acrivos, Steady long slender droplets in two-dimensional straining motion, *J. Fluid Mech.* **91**, 401 (1979).
- [13] B. Bentley and L. G. Leal, An experimental investigation of drop deformation and breakup in steady, two-dimensional linear flows, *J. Fluid Mech.* **167**, 241 (1986).
- [14] J. Rallison, A numerical study of the deformation and burst of a viscous drop in general shear flows, *J. Fluid Mech.* **109**, 465 (1981).
- [15] H. A. Stone, Dynamics of drop deformation and breakup in viscous fluids, *Annu. Rev. Fluid Mech.* **26**, 65 (1994).
- [16] V. Narsimhan and E. S. Shaqfeh, Lateral drift and concentration instability in a suspension of bubbles induced by Marangoni stresses at zero Reynolds number, *Phys. Fluids* **22**, 101702 (2010).
- [17] H. A. Stone and L. G. Leal, The effects of surfactants on drop deformation and breakup, *J. Fluid Mech.* **220**, 161 (1990).
- [18] X. Li and C. Pozrikidis, The effect of surfactants on drop deformation and on the rheology of dilute emulsions in stokes flow, *J. Fluid Mech.* **341**, 165 (1997).
- [19] Y. Pawar and K. J. Stebe, Marangoni effects on drop deformation in an extensional flow: The role of surfactant physical chemistry. I. Insoluble surfactants, *Phys. Fluids* **8**, 1738 (1996).
- [20] P. M. Kamat, B. W. Wagoner, S. S. Thete, and O. A. Basaran, Role of Marangoni stress during breakup of surfactant-covered liquid threads: Reduced rates of thinning and microthread cascades, *Phys. Rev. Fluids* **3**, 043602 (2018).
- [21] D. Langevin, Influence of interfacial rheology on foam and emulsion properties, *Adv. Colloid Interface Sci.* **88**, 209 (2000).
- [22] R. Miller, J. K. Ferri, A. Javadi, J. Krägel, N. Mucic, and R. Wüstneck, Rheology of interfacial layers, *Colloid Polym. Sci.* **288**, 937 (2010).
- [23] S. Choi, S. Steltenkamp, J. A. Zasadzinski, and T. Squires, Active microrheology and simultaneous visualization of sheared phospholipid monolayers, *Nat. Commun.* **2**, 1 (2011).
- [24] G. G. Fuller and J. Vermant, Complex fluid-fluid interfaces: Rheology and structure, *Annu. Rev. Chem. Biomol. Eng.* **3**, 519 (2012).
- [25] D. Barthes-Biesel, Capsule motion in flow: Deformation and membrane buckling, *C. R. Phys.* **10**, 764 (2009).
- [26] X. Li, D. Barthes-Biesel, and A. Helmy, Large deformations and burst of a capsule freely suspended in an elongational flow, *J. Fluid Mech.* **187**, 179 (1988).
- [27] K.-S. Chang and W. L. Olbricht, Experimental studies of the deformation and breakup of a synthetic capsule in steady and unsteady simple shear flow, *J. Fluid Mech.* **250**, 609 (1993).
- [28] T. Verwijlen, P. Moldenaers, and J. Vermant, A fixture for interfacial dilatational rheometry using a rotational rheometer, *Eur. Phys. J.: Spec. Top.* **222**, 83 (2013).
- [29] C. F. Brooks, G. G. Fuller, C. W. Frank, and C. R. Robertson, An interfacial stress rheometer to study rheological transitions in monolayers at the air-water interface, *Langmuir* **15**, 2450 (1999).
- [30] A. P. Gunning, A. R. Kirby, P. J. Wilde, R. Penfold, N. C. Woodward, and V. J. Morris, Probing the role of interfacial rheology in the relaxation behaviour between deformable oil droplets using force spectroscopy, *Soft Matter* **9**, 11473 (2013).
- [31] P. Erni, Deformation modes of complex fluid interfaces, *Soft Matter* **7**, 7586 (2011).

- [32] R. W. Flumerfelt, Effects of dynamic interfacial properties on drop deformation and orientation in shear and extensional flow fields, *J. Colloid Interface Sci.* **76**, 330 (1980).
- [33] R. Cox, The deformation of a drop in a general time-dependent fluid flow, *J. Fluid Mech.* **37**, 601 (1969).
- [34] J. Gounley, G. Boedec, M. Jaeger, and M. Leonetti, Influence of surface viscosity on droplets in shear flow, *J. Fluid Mech.* **791**, 464 (2016).
- [35] W. J. Phillips, R. W. Graves, and R. W. Flumerfelt, Experimental studies of drop dynamics in shear fields: Role of dynamic interfacial effects, *J. Colloid Interface Sci.* **76**, 350 (1980).
- [36] M. J. Boussinesq, Sur l'existence d'une viscosité superficielle, dans la mince couche de transition séparant un liquide d'un autre fluide contigu, *Ann. Chim. Phys.* **29**, 349 (1913).
- [37] L. Scriven, Dynamics of a fluid interface equation of motion for Newtonian surface fluids, *Chem. Eng. Sci.* **12**, 98 (1960).
- [38] V. Narsimhan, The effect of surface viscosity on the translational speed of droplets, *Phys. Fluids* **30**, 081703 (2018).
- [39] D. Langevin, Rheology of adsorbed surfactant monolayers at fluid surfaces, *Annu. Rev. Fluid Mech.* **46**, 47 (2014).
- [40] H. Manikantan and T. M. Squires, Pressure-dependent surface viscosity and its surprising consequences in interfacial lubrication flows, *Phys. Rev. Fluids* **2**, 023301 (2017).
- [41] O. Manor, O. Lavrenteva, and A. Nir, Effect of non-homogeneous surface viscosity on the Marangoni migration of a droplet in viscous fluid, *J. Colloid Interface Sci.* **321**, 142 (2008).
- [42] A. Williams and A. Prins, Comparison of the dilational behaviour of adsorbed milk proteins at the air-water and oil-water interfaces, *Colloids Surf., A* **114**, 267 (1996).
- [43] K. A. Erk, J. D. Martin, J. T. Schwalbe, F. R. Phelan Jr., and S. D. Hudson, Shear and dilational interfacial rheology of surfactant-stabilized droplets, *J. Colloid Interface Sci.* **377**, 442 (2012).
- [44] P. Erni, P. Fischer, E. J. Windhab, V. Kusnezov, H. Stettin, and J. Läger, Stress- and strain-controlled measurements of interfacial shear viscosity and viscoelasticity at liquid/liquid and gas/liquid interfaces, *Rev. Sci. Instrum.* **74**, 4916 (2003).
- [45] V. Narsimhan, Shape and rheology of droplets with viscous surface moduli, *J. Fluid Mech.* **862**, 385 (2019).
- [46] R. Pawlowski, A. Salinger, J. Shadid, and T. Mountziaris, Bifurcation and stability analysis of laminar isothermal counterflowing jets, *J. Fluid Mech.* **551**, 117 (2006).
- [47] J. Q. Feng and O. A. Basaran, Shear flow over a translationally symmetric cylindrical bubble pinned on a slot in a plane wall, *J. Fluid Mech.* **275**, 351 (1994).
- [48] G. Iooss and D. D. Joseph, *Elementary Stability and Bifurcation Theory* (Springer-Verlag, New York, 2012).
- [49] R. A. Brown and L. Scriven, The shapes and stability of captive rotating drops, *Philos. Trans. R. Soc. London A* **297**, 51 (1980).
- [50] Y. Yamaguchi, C. J. Chang, and R. A. Brown, Multiple buoyancy-driven flows in a vertical cylinder heated from below, *Philos. Trans. R. Soc. London A* **312**, 519 (1984).
- [51] A. Acrivos and T. Lo, Deformation and breakup of a single slender drop in an extensional flow, *J. Fluid Mech.* **86**, 641 (1978).
- [52] E. Hinch and A. Acrivos, Long slender drops in a simple shear flow, *J. Fluid Mech.* **98**, 305 (1980).
- [53] G. I. Taylor, The formation of emulsions in definable fields of flow, *Proc. R. Soc. London A* **146**, 501 (1934).
- [54] K. Feigl, D. Megias-Alguacil, P. Fischer, and E. J. Windhab, Simulation and experiments of droplet deformation and orientation in simple shear flow with surfactants, *Chem. Eng. Sci.* **62**, 3242 (2007).
- [55] T. W. Secomb and R. Skalak, Surface flow of viscoelastic membranes in viscous fluids, *Q. J. Mech. Appl. Math.* **35**, 233 (1982).
- [56] C. Pozrikidis, Effects of surface viscosity on the finite deformation of a liquid drop and the rheology of dilute emulsions in simple shearing flow, *J. Non-Newtonian Fluid Mech.* **51**, 161 (1994).
- [57] S. Torza, R. Cox, and S. Mason, Particle motions in sheared suspensions XXVII. Transient and steady deformation and burst of liquid drops, *J. Colloid Interface Sci.* **38**, 395 (1972).

- [58] F.-D. Rumscheidt and S. Mason, Particle motions in sheared suspensions XII. Deformation and burst of fluid drops in shear and hyperbolic flow, *J. Colloid Sci.* **16**, 238 (1961).
- [59] A. Acrivos, The breakup of small drops and bubbles in shear flows, *Ann. N.Y. Acad. Sci.* **404**, 1 (1983).
- [60] J. Rallison, The deformation of small viscous drops and bubbles in shear flows, *Annu. Rev. Fluid Mech.* **16**, 45 (1984).
- [61] J. Rallison and A. Acrivos, A numerical study of the deformation and burst of a viscous drop in an extensional flow, *J. Fluid Mech.* **89**, 191 (1978).
- [62] Z. Y. Luo, X. L. Shang, and B. F. Bai, Influence of pressure-dependent surface viscosity on dynamics of surfactant-laden drops in shear flow, *J. Fluid Mech.* **858**, 91 (2019).
- [63] P. Fischer and P. Erni, Emulsion drops in external flow fields: The role of liquid interfaces, *Curr. Opin. Colloid Interface Sci.* **12**, 196 (2007).
- [64] V. Cristini, S. Guido, A. Alfani, J. Bławdziewicz, and M. Loewenberg, Drop breakup and fragment size distribution in shear flow, *J. Rheol.* **47**, 1283 (2003).
- [65] J. Li, Y. Y. Renardy, and M. Renardy, Numerical simulation of breakup of a viscous drop in simple shear flow through a volume-of-fluid method, *Phys. Fluids* **12**, 269 (2000).